Potential drop monitoring of creep damage at a weld

Joseph Corcoran, Peter B. Nagy, and Peter Cawley

Citation: AIP Conference Proceedings **1706**, 170002 (2016); doi: 10.1063/1.4940625
View online: http://dx.doi.org/10.1063/1.4940625
View Table of Contents: http://scitation.aip.org/content/aip/proceeding/aipcp/1706?ver=pdfcov
Published by the AIP Publishing

Potential Drop Monitoring of Creep Damage at a Weld

Joseph Corcoran[1], Peter B. Nagy[1, 2] and Peter Cawley[1, a)]

[1]*Department of Mechanical Engineering, Imperial College London, London, UK*
[2]*Department of Aerospace Engineering & Engineering Mechanics, University of Cincinnati, Cincinnati, Ohio, USA*

[a)]p.cawley@imperial.ac.uk

Abstract. Creep failure at welds will often be the life limiting factor for pressurised power station components, offering a site for local damage accumulation. Monitoring the creep state of welds will be of great value to power station management and potential drop monitoring may provide a useful tool. This paper provides a preliminary study of potential drop monitoring of creep damage at a weldment, suggesting a measurement arrangement for a previously documented quasi-DC technique that is well suited to the application. The industrial context of the problem of creep damage at a weldment is explored, together with a numerical simulation of the effect of cracking, finally, a cross-weld accelerated creep test demonstrating the promise of the technique is presented.

INDUSTRIAL CONTEXT

Weldments in high temperature, high pressure, power station components can be generally categorised as girth or seam welds. Girth welds are those made circumferentially around the pipe and may be used to join lengths of pipe end to end or onto a header. Seam welds are made axially along the length of a component and exist to form components out of plate material. Both types have specific failure characteristics and should be considered separately. In general, seam welds are not present in high-pressure, high-temperature pipe work in Europe and therefore this paper will be predominantly concerned with girth weld failures, though many of the themes explored will be equally applicable to both.

Girth weld failures are driven by the cross-weld axial stresses arising from internal pressure and additionally the bending caused by the dead weight of the pipe. It is usually assumed that the axial stresses are much smaller than the circumferential stresses [1] and therefore girth welds tend to fail in a 'leak before break' manner. Overwhelmingly, concern around girth weld failure is associated with Type IV failure [1–5]. High chrome steels are known to be particularly susceptible and the widespread adoption of P91 material means that there is considerable concern in the power industry at present [1, 2, 6, 7]. Type IV damage accumulates in the intercritical heat-affected zone (ICHAZ) of a weld, a narrow band of material located at the edge of the HAZ adjacent to the parent material as shown in Fig. 1. The ICHAZ is rendered creep 'soft' by the prior thermal exposure of the welding process; the 850-900 °C temperature at that location is such that the grain structure is refined and carbides are significantly coarsened [4].

Although Type IV cracking in girth welds is associated with bending stresses that are higher at the pipe outside surface, crack initiation is believed to initiate sub-surface at the near outer diameter region. Specifically, cracks are expected to initiate at a depth of the first weld bead below the surface weld pass; this is a result of the surface temper bead and the tendency for cavitation to occur on the more radially orientated interface [3, 8]. It is understood that the approximate depth of the second weld bead is ~2-10 mm depending on the preparation of the weld cap [9].

Type IV weld failure is understood to be characterised by the accumulation of grain boundary separation leading to microcracking in the ICHAZ but also locally high strain rates which may serve as a precursor to crack initiation; both of these symptoms may be monitored using the proposed potential drop technique.

42nd Annual Review of Progress in Quantitative Nondestructive Evaluation
AIP Conf. Proc. 1706, 170002-1–170002-10; doi: 10.1063/1.4940625

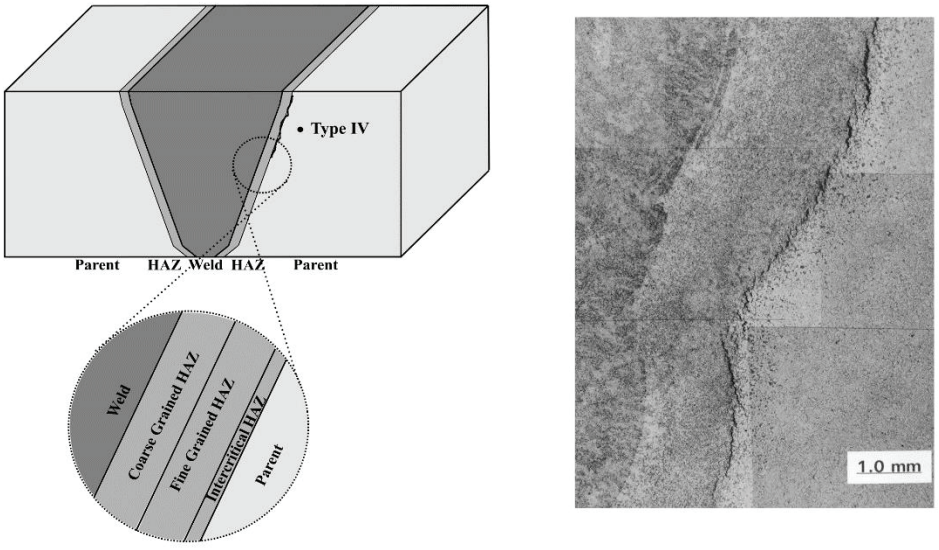

(a) (b)

FIGURE 1. (a) The macrostructure of the HAZ showing the position of the Intercritical HAZ (ICHAZ) where Type IV failure occurs. (b) Example of Type IV damage which is a common issue in girth welds [10]; reprinted from Sposito et al., *NDT and E International*, **43**, 555–567 (2010) with permission from Elsevier.

POTENTIAL DROP MONITORING

A quasi-DC potential drop monitoring system has been previously presented [11, 12] and will be used in this paper. The current penetration depth in alternating current potential drop (ACPD) measurements is usually dictated by the electromagnetic skin effect. The injected current is electromagnetically 'squeezed' to the surface of the component; the skin depth, δ, is the depth from the surface at which the current density reduces to $1/e$ (≈37%) of the surface density and can be calculated as

$$\delta = \frac{1}{\sqrt{\pi f \sigma \mu}}, \tag{1}$$

where f is the current frequency, σ is the electrical conductivity and μ is the magnetic permeability. In the ferromagnetic materials of interest the magnetic permeability is known to vary depending on temperature, local alloy composition, stress, cold work and weld history [13]. Variation in magnetic permeability will therefore influence the skin depth and, in turn, the measured resistance, undermining the stability of the measurement. For this reason a quasi-DC inspection current is used, usually 1-3 Hz. The use of such low frequencies ensures that the electromagnetic skin depth is sufficiently large that the current penetration is instead limited by the electrode separation, suppressing the skin effect. The use of alternating current allows phase sensitive detection, offering a greatly improved signal to noise ratio.

A square configuration of electrodes is adopted for enhanced strain sensitivity and directional sensitivity to anisotropic defects which are characteristic of creep damage. Two sequential orthogonal resistance measurements are taken using the four electrodes, as illustrated in Fig. 2 (a).

The electrodes are permanently installed by welding wires or intermediary studs onto the component. The measurement therefore becomes sensitive to strain; as the component deforms the distances between electrodes will change, therefore influencing the measured resistance. Additionally, as grain boundary separation develops and cracking initiates, a macroscopic impediment to current flow is presented, reducing the area available for current flow and distorting the potential field. The potential drop measurement therefore has dual-sensitivity to both the anticipated localised strain and damage.

The measurement can be implemented in an array arrangement, as shown in Fig. 2 (b), allowing local variations to be detected and providing contextual information. It is therefore proposed that a potential drop array is placed across

the weld interface. The local effect of strain and damage accumulation in the element straddling the heat affected zone should become evident.

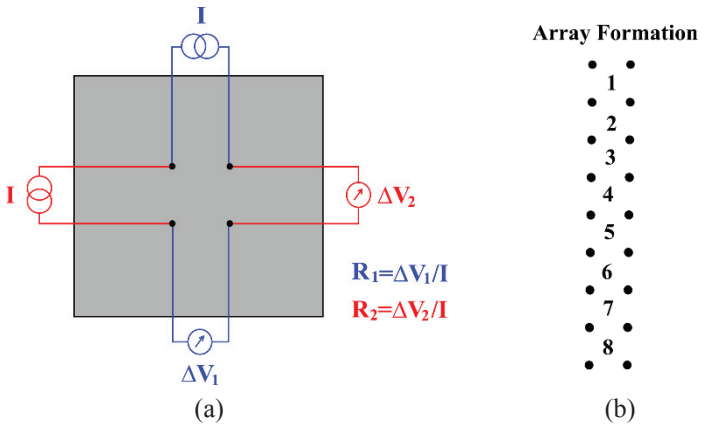

FIGURE 2. (a) A single element of the potential drop array. Two orthogonal transfer resistances are measured from the same square arrangements of electrodes. (b) An array formed from a chain of potential drop elements. It is intended that the array be placed across the weld interface to identify local accumulation of strain and damage.

It is common in potential drop measurements to take reference measurements where no defect is believed to be present to provide a measurement that can be used to compensate for resistivity changes not associated with damage. The resistivity of the component will be dominated by reversible temperature effects but will also be influenced by irreversible microstructural changes, the reference measurement can therefore be used to compensate for resistivity changes in the measurements. As it is practically difficult to implement a strain independent measurement in power station components it has been suggested that the orthogonal resistances be divided and in doing so the isotropic resistivity common to both measurements will cancel out [11] avoiding the need for a reference measurement. Additionally, this resistance ratio can be normalised to a given initial condition; this leaves a resistivity independent metric that is sensitive to strain and increase in damage and it is this that we wish to interpret. This metric will be referred to as the capitalised 'Normalised Resistance Ratio' or NRR,

$$NRR = \frac{(R_1/R_2)}{(R_{10}/R_{20})} \tag{2}$$

where the subscripts 1 and 2 denote the direction of the orthogonal measurements as indicated in Fig. 2 while the subscript 0 denotes the measurement at an initial reference condition that has been used for normalisation.

SIMULATIONS OF THE EFFECT OF CRACKING ON A SQUARE ARRANGEMENT POTENTIAL DROP MEASUREMENT

Cracking influences DC or quasi-DC potential drop measurements by reducting the available area for current flow and leasing to distortion of the potential field. It will be a function of crack size, geometry, orientation and position and therefore inversion of crack geometry is not trivial. Two examples will be presented in order to illustrate the likely influence of cracking on the potential drop measurement and the importance of crack position on sensitivity. It is important to recall that the current penetration is limited approximately to the depth of one electrode separation, this indicates that the depth of crack initiation and growth relative to the sensors field of sensitivity is an important consideration. The results will inform future optimisation for on-site applications.

Figure 3 shows schematics of two models studied using Comsol [14]. A conducting cube of 80 mm x 80 mm x 80 mm was created with a 5 mm square electrode configuration on the centre of one face, ensuring the measurements were negligibly affected by the cube edges and so the component would behave as if it were infinitely large. Point current sources and point potential probes were used to replicate a DC potential drop measurement. The two orthogonal resistances were simulated while a crack of increasing size was imposed on the model, as illustrated. The crack extends through the length of the conducting block and intersects the centre line of the electrodes; it is

acknowledged that this may not be realistic but allows an investigation into two cases of crack growth. The distinction between the two models is that in Simulation 1 the crack initiates from the top surface and grows down through the component, while in Simulation 2 the crack initiates at the bottom surface and grows towards the electrodes on the top surface. Resistance values are normalised to their values with no crack present and in Simulation 1 the crack lengths, d_a,were normalised to the electrode separation, a, and in Simulation 2 the remaining intact length, d_b (component thickness - crack length) was normalised to the electrode separation.

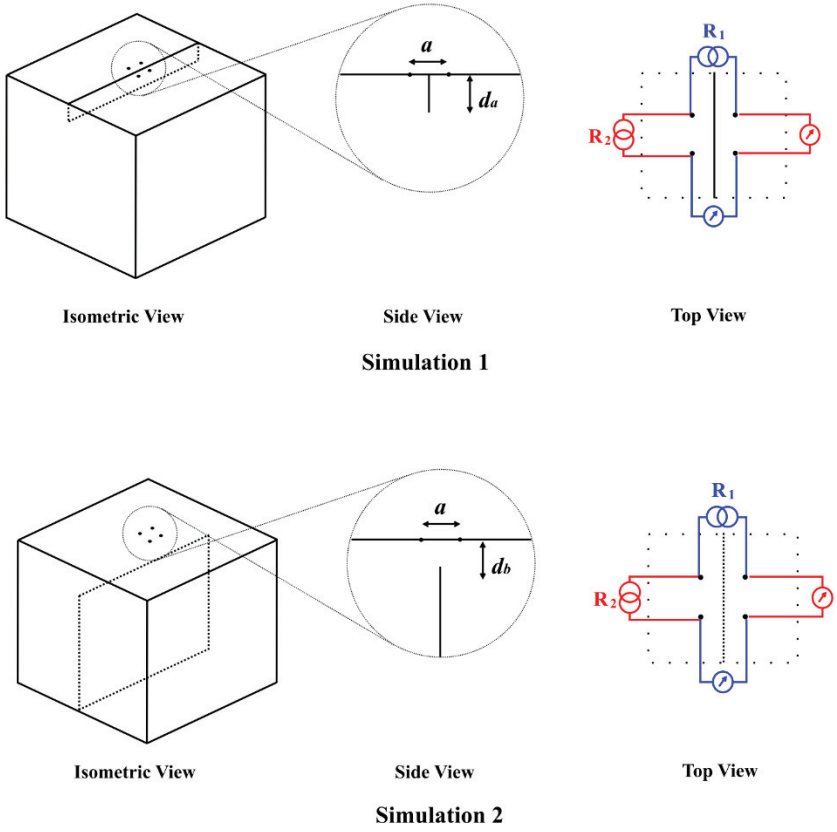

FIGURE 3. Schematics showing illustrations of the two models simulated. A sensor of 5 mm electrode separation is modelled on the top surface of a 80 mm x 80 mm x 80 mm conducting block. In both cases the crack extends across the entire width of the specimen. In Simulation 1 the crack initiates on the top surface and propagates down through the specimen. In Simulation 2 the crack initiates at the bottom of the specimen and propagates towards the top surface of the component where the sensor is placed. Resistances are described with subscript 1 and 2 indicating the orientation with respect to the crack as shown.

Simulation 1

Figure 4 shows the results from Simulation 1, the crack growing from the top surface. Initially it can be seen that there is very little sensitivity to crack growth until the crack size reaches approximately one tenth of the electrode separation with a maximum sensitivity when the crack length is approximately half the length scale of the electrode separation. The resistances taken orthogonal to the crack (in blue) will increase with crack length as the current is forced around the crack. In the parallel direction however the apparent resistance will decrease as the increasing crack depth separates the potential measuring electrodes from the current path, the potential difference and therefore the inferred transfer resistance must then decrease.

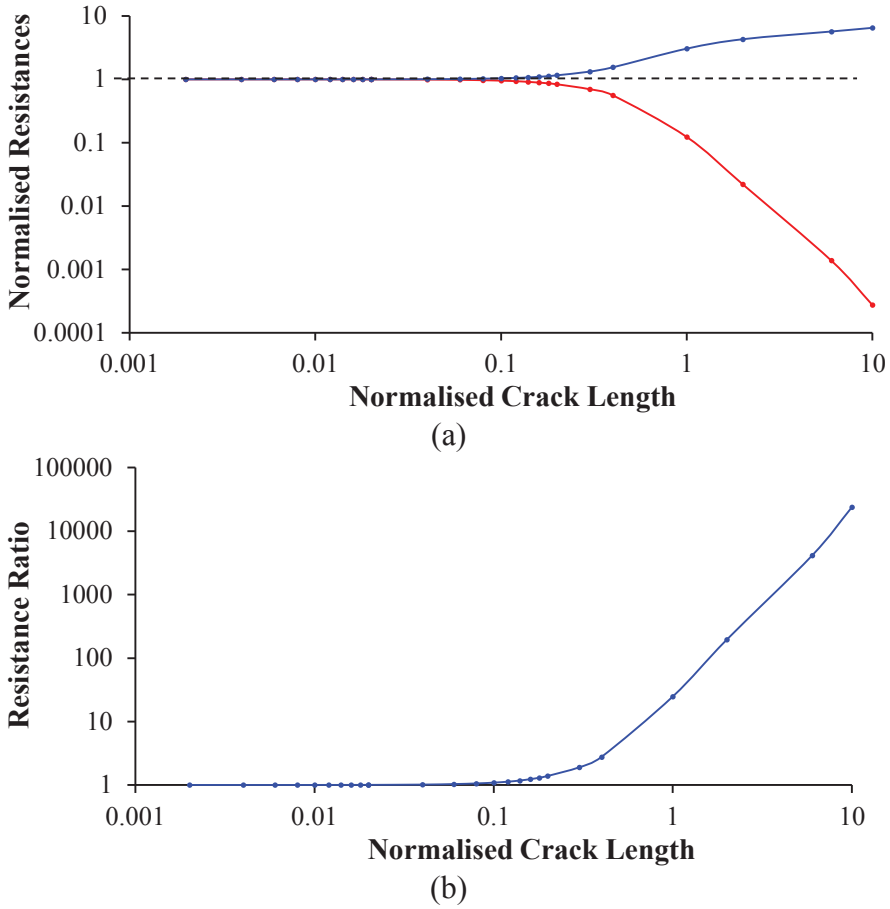

FIGURE 4. Results of Simulation 1: (a) Resistances normal and parallel to the weld/parent interface with colours according to Fig. 3. (b) The ratio of the normal and parallel resistances. The normalised crack length is the depth of the crack divided by the electrode separation.

Simulation 2

In Simulation 2 the crack is growing from the bottom of the component and the intact remaining depth normalised to the electrode separation is plotted. Figure 5 shows that sensitivity to changes in intact depth are diminishingly small at values greater than 1; as the current penetration depth is limited to approximately the electrode separation the current will not interact with a crack deeper than this. As the crack grows the resistance measured orthogonal to the crack must asymptotically approach infinity as the remaining available area decreases, eventually there will be no available cross section for current to pass. Similarly, the apparent resistance measured parallel to the crack will asymptotically approach zero as the injecting and sensing electrodes become increasingly isolated from each other.

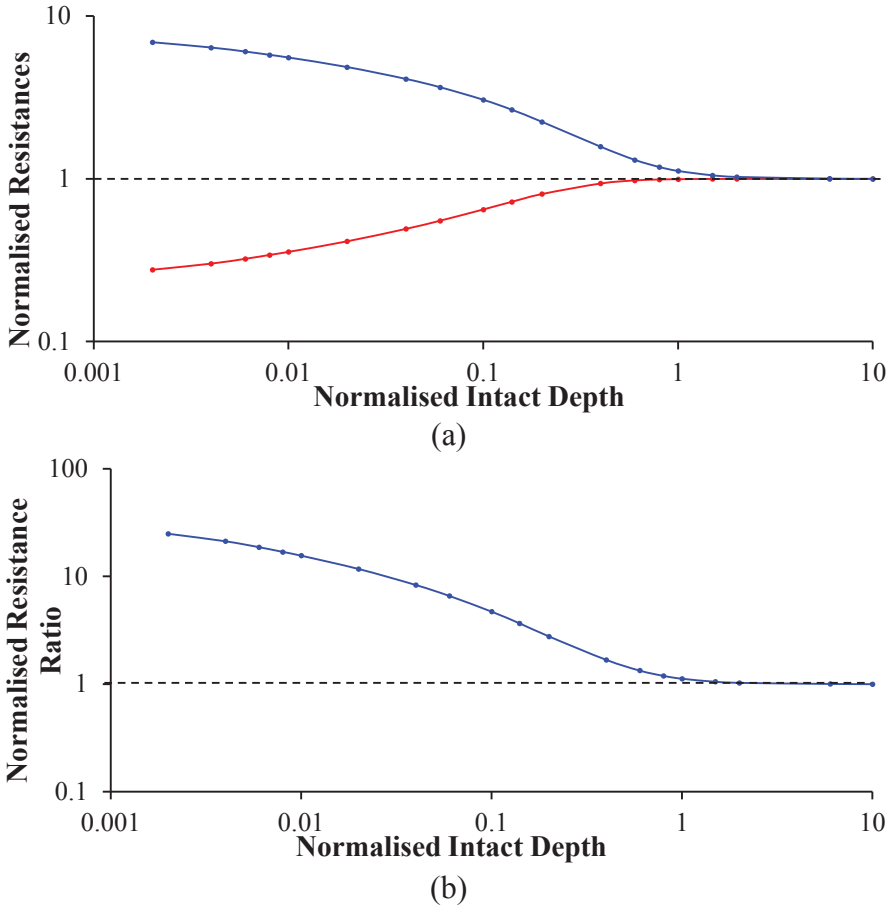

FIGURE 5. Results of Simulation 2: (a) Resistances normal and parallel to the weld/parent interface with colours according to Fig. 3. (b) The ratio of the normal and parallel resistances. The normalised intact depth is the remaining depth below the surface before the crack tip.

In both cases of crack propagation the contrasting influence on orthogonal resistances acts to amplify the sensitivity of the resistance ratio; normal to the crack the separation of injection electrodes will increase the potential between sensing electrodes increasing the transfer resistance, parallel to the crack the separation of the injection electrodes from the sensing electrodes reduces the measured potential difference and the inferred transfer resistance is reduced. These simulations present the compromise required in optimising the application of potential drop measurements for monitoring macro-defects. A larger electrode separation will increase the penetration depth and therefore the depth at which cracks may be detected. Conversely, the larger the electrode separation the smaller the defects will be relative to the measurement geometry and so sensitivity is decreased. These two simple models were used to broadly illustrate the sensitivity of the potential drop method to macroscopic damage. In reality the cracks will grow laterally as well as through the depth of the component and will not necessarily occur along the centre line of a sensor. A more in depth study of the influence of crack growth is to be completed.

ACCELERATED CROSS-WELD CREEP TEST

An accelerated creep test was conducted in order to demonstrate the use of the potential drop technique for monitoring creep damage. A cross-weld uniaxial creep specimen was manufactured from a 0.5Cr-0.5Mo-0.25V component with 2.25Cr-1Mo weld material. The specimen had a gauge cross section of 24 mm x 10 mm and length of 40 mm.

In order to identify the different domains, one surface of the cross-weld specimen was polished and a Vickers Hardness test was conducted along the length of the specimen; it was then etched to reveal microscopic features. The

results of both procedures are combined in Fig. 6. The macrograph reveals the weld parent interface and clearly shows the extent of the HAZ; also visible are the Vickers Hardness indentations. The Vickers hardness results are superimposed on to the image with a scale matching the macrographs and so values are aligned with the indentations. As expected the weld material is harder than the parent material, hardness values reach a peak in the coarse grained HAZ and reduce moving through the HAZ. It can be assumed therefore that the ICHAZ is approximately 3.5 mm from the weld face.

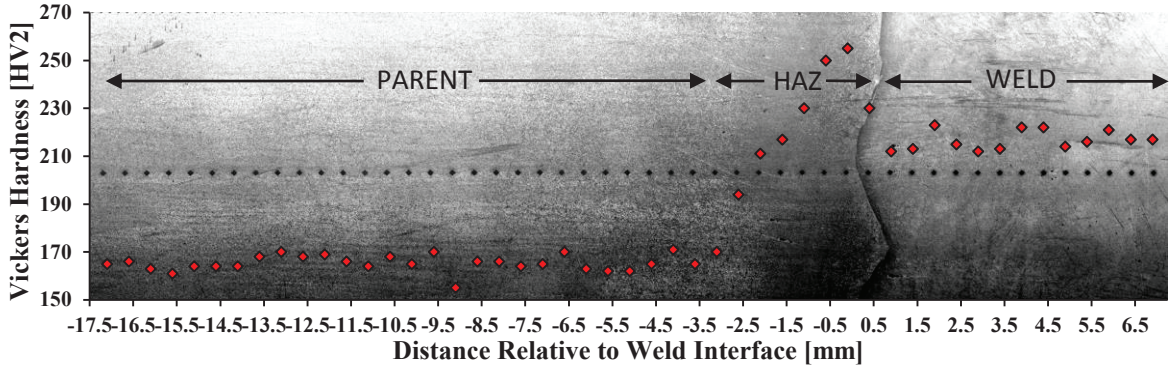

FIGURE 6. Vickers Hardness against distance along specimen. In the background a micrograph of the etched material is shown with a scale matching the x-axis of the graph. The indentations from the Vickers Hardness measurement can be seen aligned to their respective data points. The HAZ can be seen to extend from ~ -3.5 mm up to the weld face.

An array of potential drop sensors was used in order to compare the creep behaviour in the different domains and help identify the localised accumulation of damage. It was decided to centre the potential drop array approximately around the ICHAZ as shown in Fig. 7. A 9-element array of 5 mm electrode separation was used with 100 mA inspection current. The sample was crept at 625 °C and 80 MPa using a lever arm creep machine with furnace. Thermocouples were installed along the gauge length and the temperature distribution was measured to be ±1 °C, however the temperature control appeared to exhibit approximately 1 °C fluctuations with a period of ~5 hours which contributed to the minimum sensitivity of this experiment. Fig. 7 (b) shows a schematic of the sample, the relative positions of the different weld domains and a legend relating to Fig. 8 and Fig. 9.

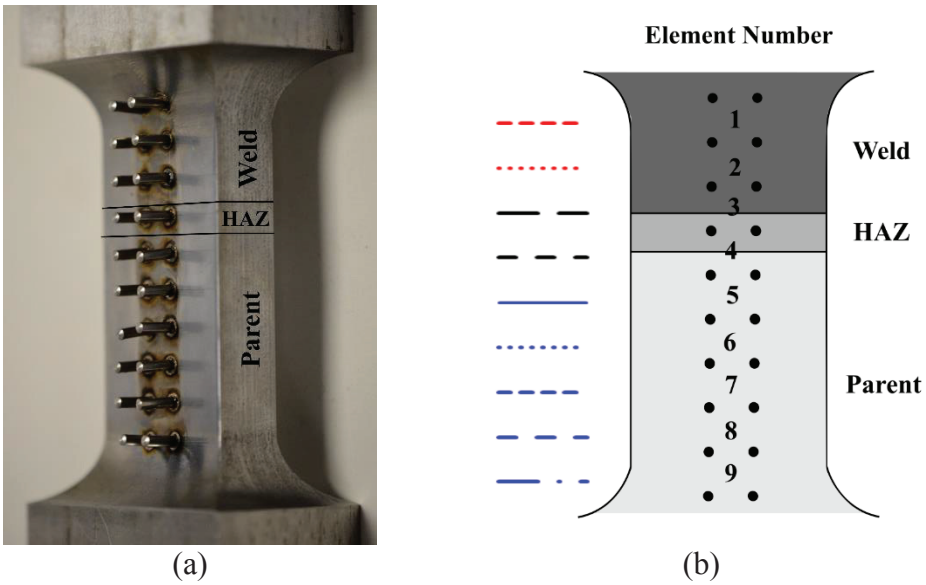

FIGURE 7. (a) Photograph of cross-weld specimen with 9-element potential drop array and approximate locations of weld domains marked. (b) Schematic of the cross-weld sample showing potential drop array, weld domains and the legend for the graphs in Fig. 8 and Fig. 9.

Figure 8 shows the Normalised Resistance Ratio over time for the experiment. Due to the combined effect of strain and cracking, inverting either is not straightforward and so will not be attempted. Instead, it is intended that the Normalised Resistance Ratio and rate of change of Normalised Resistance Ratio will provide a compound indicator of creep state. For much of the experiment resistance changes are expected to be largely attributed to strain accumulation. Although there will be different strain behaviour in the different material domains, it is important to note that there will also be a 'background' strain distribution resulting from change in geometry towards the end of the component and additionally an imperfect temperature distribution.

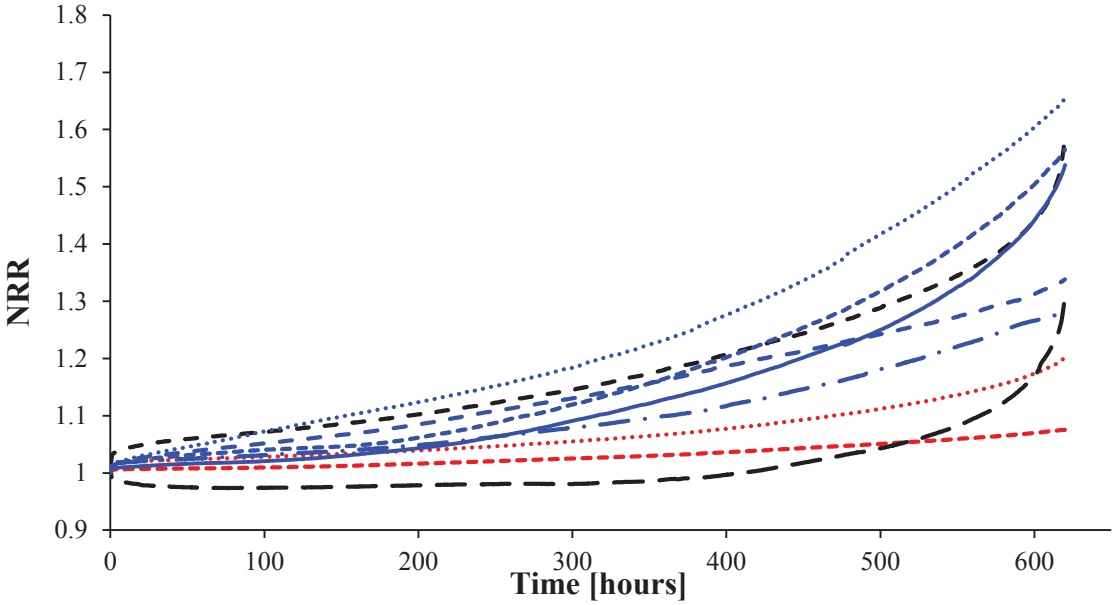

FIGURE 8. Normalised Resistance Ratio against time for cross-weld creep specimen. Normalisation was made immediately prior to loading. Legend according to Fig. 7; blue measurements are of parent material, red are weld material and black include HAZ.

The key feature of Fig.8 is the rapid increase in the rate of change of Normalised Resistance Ratio in the vicinity of the weld interface approaching failure. It is well known that increase in strain rate is a good indicator of proximity to failure; as damage accumulates in the component the creep sustaining cross section is compromised and a symptomatic increase in strain rate results in 'tertiary creep'. Likewise, clearly the rapid and substantial increase in resistance due to the presence of a crack will provide useful information on the proximity to failure.

To illustrate this more clearly Fig. 9 shows the rate of change of Normalised Resistance Ratio against time. The dashes indicating the element location have been removed as it was not possible or necessary to display them clearly. It is shown however that the measurements in the vicinity of the weld interface show a very dramatic increase towards failure. The test was aborted just before failure and indeed a macro-crack was clearly evident in the vicinity of the HAZ.

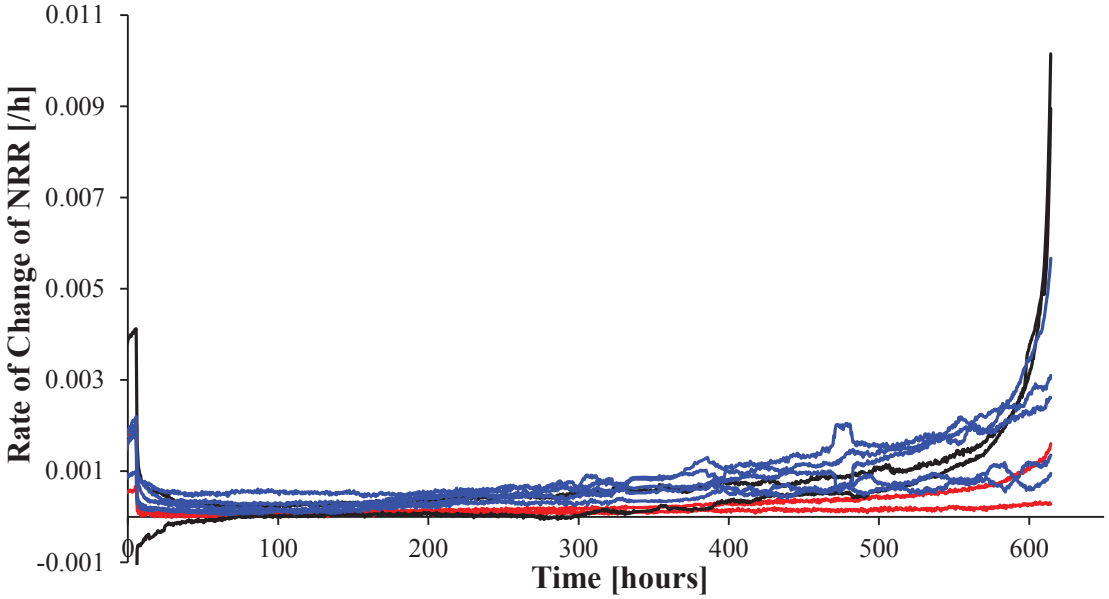

FIGURE 9. Rate of Change of Normalised Resistance Ratio against time for cross-weld creep test. Legend according to Fig. 7 but dashes have been omitted for simplicity; blue measurements are of parent material, red are weld material and black include HAZ. Rate calculated by central finite difference method with a time step of 10 hours.

This experiment demonstrates the sensitivity of potential drop methods to the macroscopic creep damage associated with weld failure. The limitation of this experiment, however, is that the component thickness was only twice the electrode separation; the crack is therefore constrained to grow within the field of sensitivity of the potential drop measurement. In thicker components it is possible, though unexpected, for a crack to initiate below the penetration depth of the potential drop measurement and considerable growth may occur before detection. Investigating the risk of this situation arising and optimising the electrode separation to account for variability in the depth of initiation is future work.

CONCLUSIONS

An implementation of a potential drop monitoring technique that is well suited to the detection of creep damage has been suggested. The use of a quasi-DC inspection frequency suppresses the influence of the electromagnetic skin effect that would otherwise undermine the stability of the measurement in the ferromagnetic materials of interest. The use of even low frequency measurements allows phase sensitive detection and greatly enhanced noise performance. A square arrangement of electrodes allows two orthogonal resistances to be measured. It provides enhanced strain sensitivity and allows the suppression of resistivity changes by dividing the two resistances. Further, it is shown in this paper that macroscopic damage dividing a sensor will have contrasting influence on the orthogonal resistance measurements; separation of the injecting electrodes will increase the potential difference measured between sensing electrodes, while separation of the injecting electrodes from the sensing electrodes will reduce the potential difference. This manifests as substantial changes in the ratio of the two resistances.

An accelerated cross-weld creep test has been completed with a potential drop array installed. The use of an array provides improved spatial information on the different material domains of the weld. This contextual information can help the identification of localised damage. The initiation and growth of cracking is clearly evident in the experimental data. Monitoring the rate of change of the resistance ratio provides an improved indicator of proximity to failure.

REFERENCES

1. H. Cerjak and P. Mayr, "Creep Strength of Welded Joints of Ferritic Steels." in *Creep Resistant Steels*, edited by F. Abe, T.-U. Kern, & R. Viswanathan (Woodhead Publishing Limited, Cambridge, 2008) pp. 472–503.
2. D. J. Abson and J.S. Rothwell, *International Materials Reviews*, **58**, 437–473. (2013)
3. F.V. Ellis, "Review of Type IV Cracking in Piping Welds", *EPRI Report TR-108971*. (1997)
4. I. J. Perrin, and D.R. Hayhurst, *International Journal of Pressure Vessels and Piping*, **76**, 599–617. (1999)
5. R. Viswanathan, and J. Stringer, *Journal of Engineering Materials and Technology*, **122**, 246-255 (2000).
6. I.A. Shibli and K. Coleman, Public Report: "Failures of P91 Steel at the West Burton Plant in England Raise Concerns About the Long Term Behaviour of the Advanced Steel". (2006)
7. "Safety and reliability concerns with P91 pressure vessels and piping." in *TWI Connect, No. 156*. (TWI Ltd., Cambridge, 2008)
8. S. Brett, "Cracking Experience in Steam Pipework Welds in National Power." In *Conference Proceeding on Materials and Welding Technology in Power Plants*. (VGB, Essen, Germany, 1994).
9. A.H. Yaghi, T.H. Hyde, A.A. Becker, and W. Sun. *Science and Technology of Welding and Joining*, **16**, 232–238 (2011).
10. G. Sposito, C. Ward, P. Cawley, P.B. Nagy and C. Scruby. *NDT and E International*, **43**, 555–567 (2010).
11. Madhi, E., & Nagy, P. B. *NDT and E International*, **44**, 708–717 (2011).
12. J. Corcoran, P. Cawley, and P.B. Nagy. "A potential drop strain sensor for in-situ power station creep monitoring." In *Review of Progress in Quantitative Nondestructive Evaluation, Eds. D. E. Chimenti, L. J. Bond and D. O. Thompson*, AIP Conference Proceedings, **1581,** 1482–1487, 2014.
13. D.C. Jiles, *Introduction to Magnetism and Magnetic Materials*, Second Edition. (Chapman & Hall/CRC, Boca Raton, 1998)
14. Comsol, Comsol Inc. (2012).